Manuscript submitted to: Volume 1, Issue 2, 87-102.
*AIMS Materials Science* DOI: 10.3934/matersci.2014.2.87
Received date 19 February 2014, Accepted date 27 March 2014, Published date 6 April 2014

*Research Article*

# Synthesis and properties of SiNx coatings as stable fluorescent markers on vertically aligned carbon nanofibers

**Ryan Pearce [1], Timothy McKnight [2], Kate L. Klein [4], Ilia N. Ivanov [3], Dale Hensley [3], Harry Meyer III [5] and Anatoli Melechko [1,*]**

[1] Materials Science and Engineering Department, North Carolina State University, NC27695, USA
[2] Measurement Sciences and Systems Engineering Division, Oak Ridge National Laboratory, Oak Ridge, TN 37831-6006, USA
[3] Center for Nanophase Materials Sciences, Oak Ridge National Laboratory, Oak Ridge, TN 37831-6488, USA
[4] University of the District of Columbia, Washington, DC 20008, USA
[5] Materials Science and Technology Division, Oak Ridge National Laboratory, Oak Ridge, TN 37831, USA

* **Correspondence:** Email: a.melechko@gmail.com

**Abstract:** The growth of vertically aligned carbon nanofibers (VACNFs) in a catalytic dc ammonia/acetylene plasma process on silicon substrates is often accompanied by sidewall deposition of material that contains predominantly Si and N. In fluorescent microscopy experiments, whereby VACNFs are interfaced to cell and tissue cultures for a variety of applications, it was observed that this material is broadly fluorescent. In this paper, we provide insight into nature of these silicon/nitrogen in-situ coatings. We propose a potential mechanism for deposition of $SiN_x$ coating on the sidewalls of VACNFs during PECVD synthesis and explore the origin of the coating's fluorescence. It is most likely that the substrate reacts with process gases similar to reactive sputtering and chemical vapor deposition (CVD), forming silane and other silicon bearing compounds prior to isotropic deposition as a $SiN_x$ coating onto the VACNFs. The formation of Si-nanoclusters (NCs) is also implicated due to a combination of strong fluorescence and elemental analysis of the samples. These broadly luminescent fibers can prove useful as registry markers in fluorescent cellular studies and for tagging and tracing applications.

**Keywords:** carbon nanofibers; plasma processing; sputtering; thin film deposition; photoluminescence; silicon nitride

## 1. Introduction

It is reported that under some synthesis parameters a silicon nitride coating forms on the sidewalls and at the base of vertically aligned carbon nanofibers (VACNFs) during plasma enhanced chemical vapor deposition (PECVD) synthesis [1-5]. The conical shape of VACNFs, as captured using scanning electron microscopy image in Figure 1, is due to $SiN_x$ sheathing layer as shown in transmission electron microscopy images in Figure 2. This coating has proven useful for enhancing mechanical properties and biocompatibility [6]. The increased mechanical properties stem from changing the fiber structure to a more conical shape in comparison to the cylindrical shape of unsheathed carbon-rich VACNFs. Some of the benefits of this coating include the ability of fibers to withstand being pressed into tissue many times without mechanical degradation [3] and sufficient rigidity to undergo many post-processing steps such as spincasting without collapse [3,6,7]. $SiN_x$ nano-layers have been shown as promising in photovoltaics as surface passivation [8,9]. In one study, the source of the $SiN_x$ sheathing was a thin sacrificial Si layer on the underlying substrate [2]. A different study used drop cast Si microparticles that redeposited onto the VACNFs during synthesis [6]. However, in all of these instances, the only source of silicon was either the bulk substrate or a layer added to the substrate. It was never as a silicon bearing gas, such as silane. VACNFs are conventionally grown from a combination of two gases, a carbon source and a nitrogenous etchant, most typically acetylene and ammonia, respectively. The coating forms during PECVD synthesis through redeposition of any present silicon in combination with nitrogen from ammonia. This $SiN_x$ coating is a by-product of a complex interplay of plasma surface interactions as it is yet to be fully analyzed [10]. The coating can also be fluorescent in the visible spectrum, making it potentially useful for biomarking in cellular interfacing studies, including impalefection, a technique employing VACNFs and other high aspect ratio structures for macromolecular delivery into cells and tissue [11]. Herein is proposed a deposition mechanism for the $SiN_x$ coating to the VACNF sidewalls as well as exploration of the photoluminescent properties of the coating.

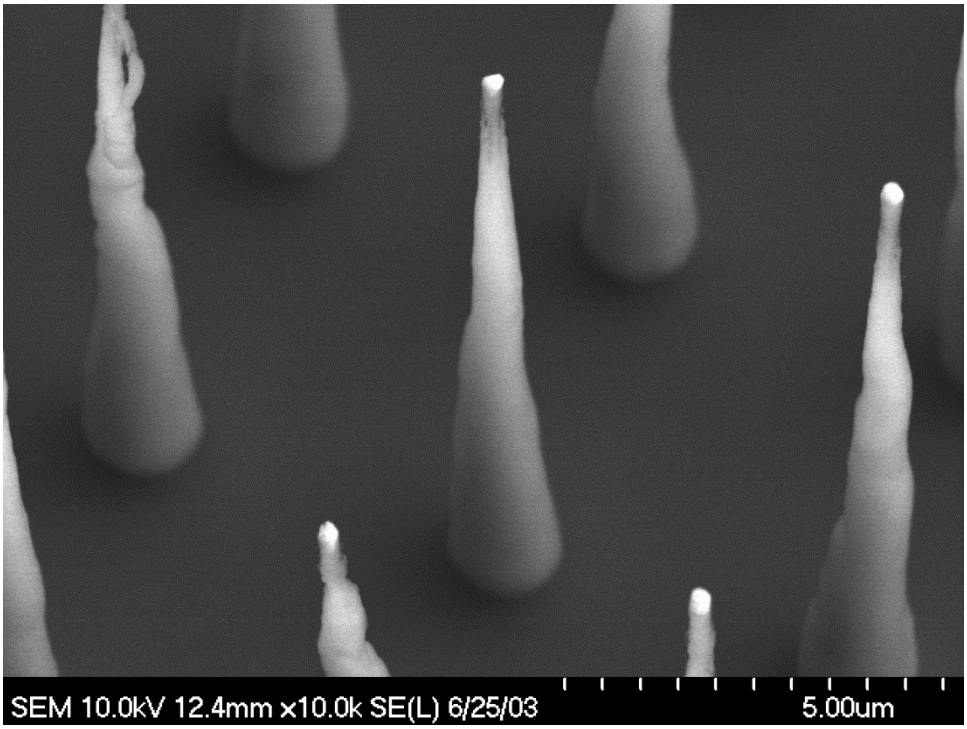


**Figure 1. SEM image of an array of vertically aligned carbon nanofibers synthesized on Si substrate with SiNx coating. A portion of an uncoated carbon nanofiber is extending from SiNx sheath by about 500 nm at the tip of each fiber.**

## 2. Materials and Method

### *2.1. VACNF Synthesis*

Vertically aligned carbon nanofibers were synthesized on n-type <100> Si wafers. Dots 2μm in diameter were photo-lithographically patterned onto the wafers. A 50 nm thick nickel catalyst layer was then deposited via electron beam evaporation and liftoff was performed to remove the nickel everywhere except for the previously defined dot pattern. The nanofibers were grown in a custom-built dc-PECVD chamber. The growth parameters for the VACNFs that were used for the fluorescence measurements were 60-sccm $C_2H_2$, 100 sccm $NH_3$, 10 Torr, 658 °C, and 3A for 10 min. The fibers that underwent Auger depth profiling were grown at 700 °C with 80 sccm $NH_3$, 40 sccm $C_2H_2$, 3 Torr, 350 mA, for 1 hour. In depth explanation of VACNF synthesis can be found elsewhere [12-15].

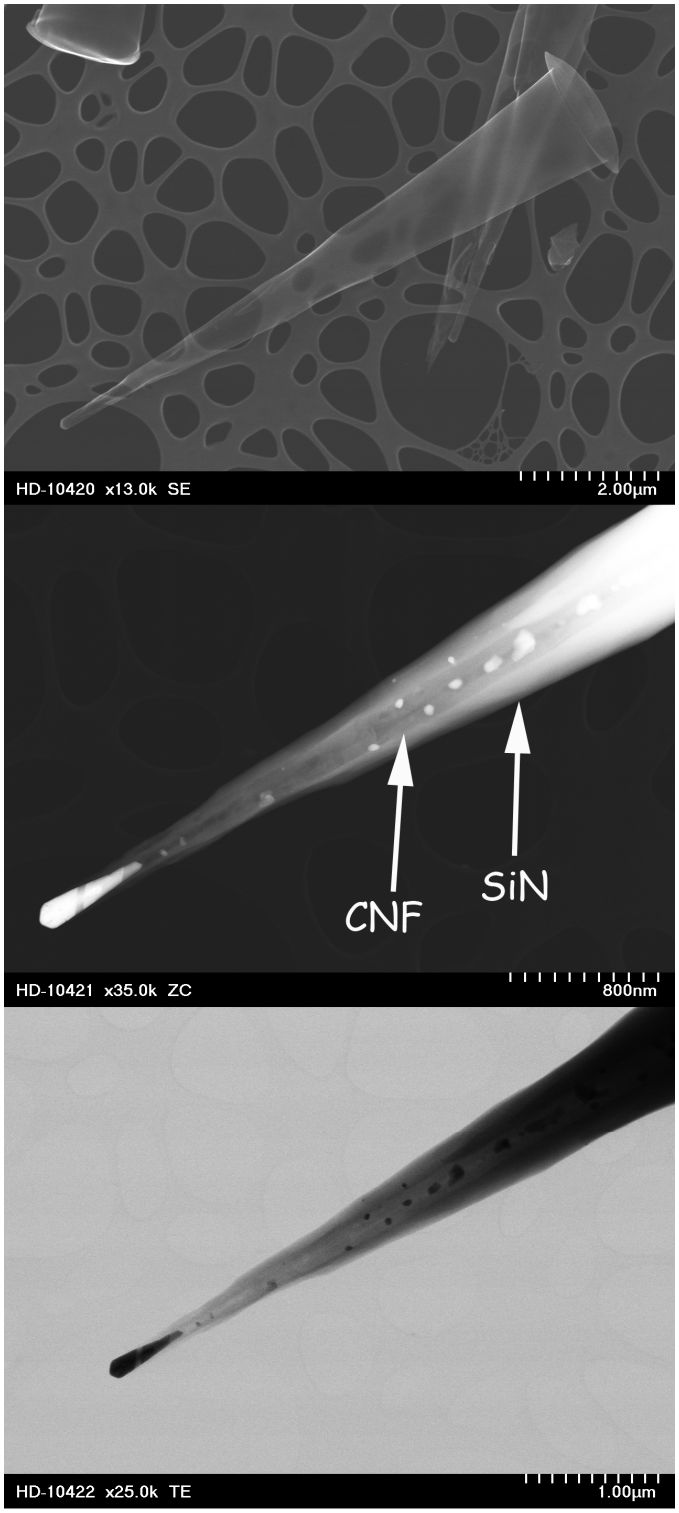


**Figure 2. TEM image of a VACNF coated with $SiN_x$. The initial stages of the film growth at the freshly form carbon nanofiber surface can be observed near the tip. a) Secondary electron mode showing surface of the nanofiber b) Z-contrast mode showing contrast between carbon core and SiN coating c) transmission mode displaying contrast between CNF and $SiN_x$ coating.**

A PECVD deposited $SiN_x$ reference film was deposited on a separate p-type <100> Si wafer using an Oxford Instruments Plasmalab 100 PECVD system. The growth parameters were 400 sccm of 5 % $SiH_4$/Ar, 20 sccm of $NH_3$, and 600 sccm of $N_2$ at 650 mT and 350 °C for 17 minutes, resulting in a film 115 nm thick.

### *2.2. Characterization*

Characterization of the resultant fibers included optical measurements, imaging, and chemical analysis. Photoluminescence mapping was performed using a Spex Fluorolog 2 at room temperature over an excitation range of 300–500 nm and an emission range of 350–700 nm. Additionally, fluorescence microscopy in a Leica TCS SP2 MP laser scanning confocal system was used to comparatively assess photobleaching of the $SiN_x$ coating against transiently expressed fluorescent proteins. EDX was used extensively along with auger electron spectroscopy (AES) depth profiling to determine chemical composition. EDX and SEM imaging was done using a Zeiss Merlin SEM with a Bruker EDX system. AES was performed using a PHI 680 Scanning Auger Nanoprobe.

## 3. Results and Discussion

### *3.1. Deposition Mechanism*

There are two primary mechanisms as to how the $SiN_x$ coating forms; either the silicon is sputtered from the substrate to the sidewalls of the fiber, or hydrogen volatilizes silicon from the substrate creating silane and other compounds in the plasma whereupon it further reacts with nitrogen from the ammonia and is redeposited through CVD processes. It has been shown that it is possible to form $SiN_x$ films using rf magnetron sputtering by using a silicon target with argon and ammonia process gases [16]. However, the amount of power supplied to the system is much greater than in a PECVD chamber. Additionally the deposition pressures are usually lower, meaning the particles in the system experience fewer collisions and retain more of their energy before impacting the substrate or target. It seems unlikely that the ions and gas molecules in a PECVD chamber would acquire the energy necessary to physically knock out many Si atoms from the substrate.

PECVD deposition of silicon nitride is also well established as previously mentioned. However, films deposited via PECVD use a silicon bearing gas, such as silane, as a silicon source, instead of the substrate itself. The silane decomposes and combines with nitrogen (usually from ammonia) on the surface of the substrate.

The films formed on VACNFs differ from both of these techniques in several ways. The largest difference is the films formed on VACNFs are being formed on three dimensional structures that are continuously growing during deposition instead of on a planar surface that exists before deposition begins. Additionally, for the work presented here, the source of silicon is only from the substrate, as

opposed to sputtering and PECVD $SiN_x$ films which use a target or a silicon bearing gas respectively. Figure 3 shows the possible mechanisms of deposition. It is important to note that sputtering usually occurs at very low pressures, around $10^{-5}$ Pa which correlates to a mean free path of ~$10^4$ m. The synthesis of VACNFs however, takes place at hundreds to thousands of Pa. A growth at 4 Torr has a mean free path of roughly only 100 μm. A significantly lower mean free path indicates that it is likely that any sputtered Si atom would undergo collisions with the other process gases and react with it, leading to a more CVD-like deposition. Alternatively, excited hydrogen molecules could react with the substrate and become subsequently volatilized, further reacting with the process gases and resulting in the $SiN_x$ film. It is possible that a combination of these two processes is what is occurring to deposit the film.

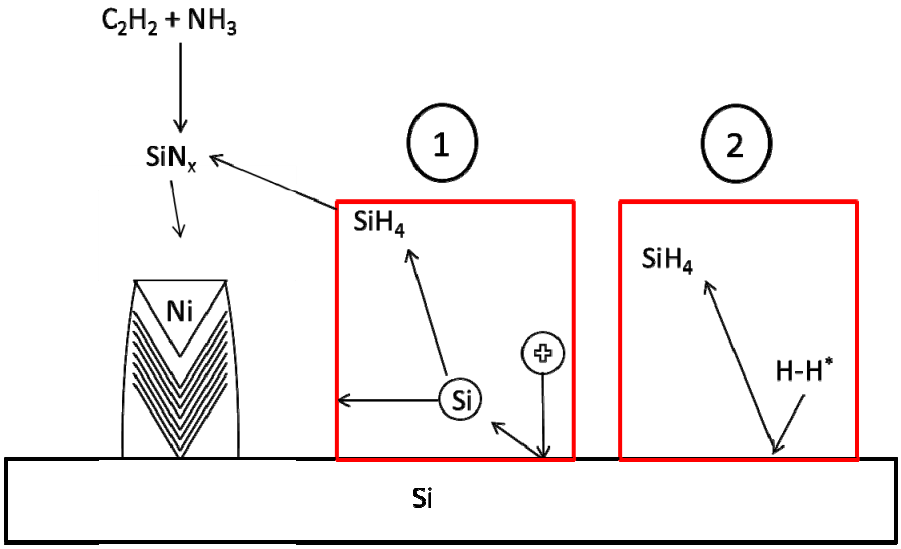


**Figure 3. Illustration of possible deposition mechanisms of $SiN_x$ coating to VACNF sidewalls (1) Reactive sputtering where ions eject Si atoms from the substrate which go on to react with the gas or (2) Excited hydrogen chemically reacts with the substrate and then volatilizes to further react through CVD processes.**

*3.2. Photoluminescence properties of SiN-coated VACNFs*

In the literature there is a large ongoing debate on the origin of the photoluminescence observed in $SiN_x$ films. There is a substantial body of work indicating the presence of Si nanoclusters (NCs) in Si-rich $SiN_x$ films [17-27]. Many of these studies attribute the photoluminescence of the films to quantum confinement effects (QCE) [23,27-30]. According to the QCE model, the photoluminescence (PL) peak is inversely proportional to the square of the average size of the Si-NCs, while intensity increases with NC density and improved passivation [17]. Others attribute the PL to the presence of defect-related states, such as nitrogen defects or Si dangling bonds [31].

Another study surmised that the blue, green, and red components of the PL were due to defects, bandtail recombination, and QCE respectively [32]. $SiN_x$ films without any Si-NCs have also been studied, with the PL in those samples being attributed to bandtail recombination [24]. It seems that the Si-NCs do not spontaneously form during co-sputtering of Si and $Si_3N_4$ targets or with some PECVD parameters and require annealing of more than 1000 °C to form the nanostructures [24,27]. Yet, it appears that growths that encourage an *a*-$SiN_x$: H matrix yield *in-situ* formatting of Si-NCs.

We observe a strong PL response from $SiN_x$ coated VACNFs as shown in Figure 4. There appear to be two emission peaks at 416 nm and 432 nm for both the PECVD $SiN_x$ coating and the VACNF coating with an excitation wavelength of 380 nm. Figure 5 shows the PL spectra for 380 nm excitation for both samples. It is possible that this dual peak stems from the presence of a bimodal size distribution of Si-NCs. From Figure 5 it can be observed that the intensity of the sample with VACNFs coated with $SiN_x$ has nearly twice the intensity of the flat PECVD $SiN_x$ film, though this could be due to there simply being a greater amount of material present on the VACNFs, which seems unlikely. Here we will make the argument that this PL response is due to the presence of Si-NCs. First, it is important to show the plausibility of Si-NCs forming. As was previously mentioned, both annealing and high hydrogen content have shown the ability to yield Si-NCs. Since the samples are grown at 700 °C in the presence of $C_2H_2$ and $NH_3$, both of these conditions are met. Another key factor is that for the synthesis of Si-NCs, the film must be Si-rich, that is that Si/N ratio is greater than stoichiometric $Si_3N_4$. Table 1 shows that the coating is in fact Si-rich, lending further credibility to the presence of Si-NCs.

**Table 1. Relative atomic concentrations in VACNF $SiN_x$ coating.**

| Element | Atomic % |
|---|---|
| Si | 41.07 |
| N | 45.75 |
| C | 7.86 |
| O | 5.33 |

Figure 6 shows an EDS line scan of a broken VACNF with a $SiN_x$ coating. From this line scan it can be seen that many nitrogen troughs are accompanied by silicon peaks, while the inverse is never true. It can be inferred then, that these Si peaks are areas where Si-NCs are present. The lack of nitrogen peaks accompanied by silicon troughs is expected, since nitrogen does not have a crystallographic structure at room temperature. The evidence for Si-NCs is further corroborated by the EDS maps shown in Figure 7. From the EDS maps of the same fiber shown in Figure 6, it can be seen that there are areas where there are bright Si clusters.

Perhaps the most convincing proof of the presence of Si-NCs is shown in Figure 8. Auger electron spectroscopy not only reveals elemental composition, but also bonding state of atoms.

Combined with ion milling, AES is a very powerful tool for elemental analysis of samples. From Figure 8 it can be seen that there is a significant amount of Si that is bonded to either O or N, and that after ~1000 μm there is only Si bonded Si, indicating that the substrate has been reached by the probe. It is critical to note that Si bonded Si is in abundance throughout the area probed, well above the substrate, alongside the O- and N- bonded Si. Some of this Si is probably bonded to the carbon that is present to form SiC, since AES only shows bonding states of atoms with significantly different electronegativities. However, there is a much greater amount of "unbonded" Si than C, so even if the full amount of present C is used to form SiC, there is still a large amount of Si that must be bonded to Si. These Si-Si bonds must invariably lead to small Si-NCs.

Now that the presence of Si-NCs and strong fluorescence of $SiN_x$ coated fibers has been established, we provide example of how this characteristic can have application. VACNF arrays have been reported extensively as a mechanical means for gene delivery into cells and tissue using a method whereby sparse arrays of nanofibers are modified with DNA and pressed into cellular matrices, resulting in widescale cellular penetration and 'microinjection' of genetic material; aka 'impalefection' [1]. An attractive advantage of this gene delivery technique is the ability of nanofibers to achieve nuclear penetration, as observed using freeze fracture and scanning electron microscopy. Nuclear penetration enables the delivery of transgene cargo directly to the transcriptional control center of the cell, thereby resulting in potentially very rapid transgene expression [33,34]. In previous optical microscopy studies, the nuclear presence of nanofibers has been difficult to characterize due to the lack of optical emission from the nanofibers [11]. Inherently fluorescent fibers thus provide advantage for imaging the presence of nanofibers within cells and tissue and potentially as registry markers for a variety of fluorescent cellular studies, particularly for confocal microscopy where there is value of a registry mark that extends through the depth of the scanned field. Figure 9 shows a vertical slice of a cell undergoing mitosis following nanofiber mediated gene delivery of DNA-constructs encoding GFP-tubulin and H2B-DsRed (monomer). Imaging was performed on a Leica SP1 laser scanning confocal microscope after impaling cells onto a periodic array of DNA-modified nanofibers at a ten micron pitch. In the image, the GFP-tubulin is largely collected within the mitosing-cell's spindle apparatus and is observed via 488 laser excition and emission collected from 510–520 nm. The condensed chromatin is observed due to the 600–655 nm emission via 458 nm laser excitation of the fluorescently labeled protein H2B-DsRed, whereby H2B is one of the 5 main histone proteins involved in the structure of chromatin in eukaryotic cells. The broad emission from the $SiN_x$-coated VACNFs stems solely from the fluorescent $SiN_x$ coating. Since the VACNFs emit over such a broad spectrum, they can be used as positional markers or "registry" marks throughout the visible spectrum. During these studies, the fluorescently labeled proteins were rapidly photobleached by the laser excitation, even though the laser was mechanically set at its lowest available power. However, the nanofiber emission remained stable. Figure 10 shows a plot of the emission intensity across the two emission ranges (same as Figure 9) as a function of time. It is observed that the emission from the fluorescently-labeled

proteins, GFP-Tubulin and H2B-DsRed decreases over time, but comparatively the intensity of the emission from VACNFs is unchanged over the time period evaluated. Therefore, in addition to emitting over a broad range, the fluorescence of the VACNFs does not photobleach, wherein the intensity of emission decreases over time due to the presence of intermediate energy levels with long half-lives.

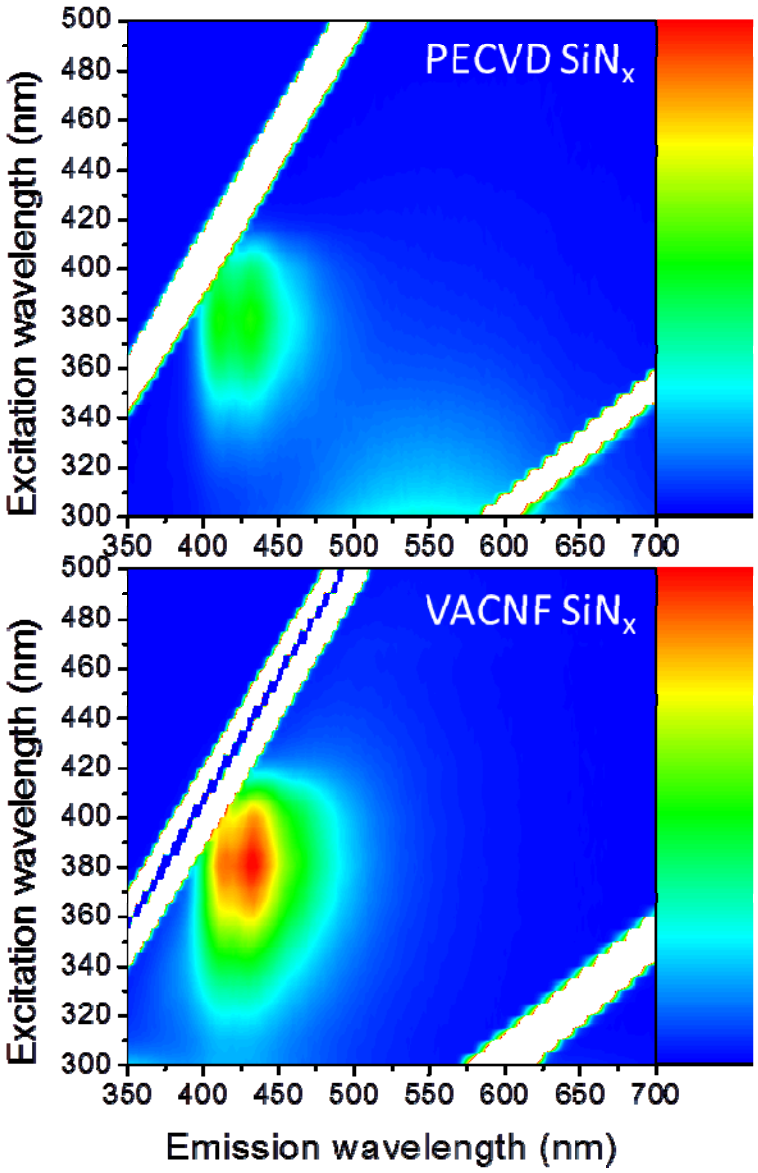


**Figure 4. Fluorescent response from a PECVD $SiN_x$ coating (top) and from a $SiN_x$ coated VACNF array (bottom).**

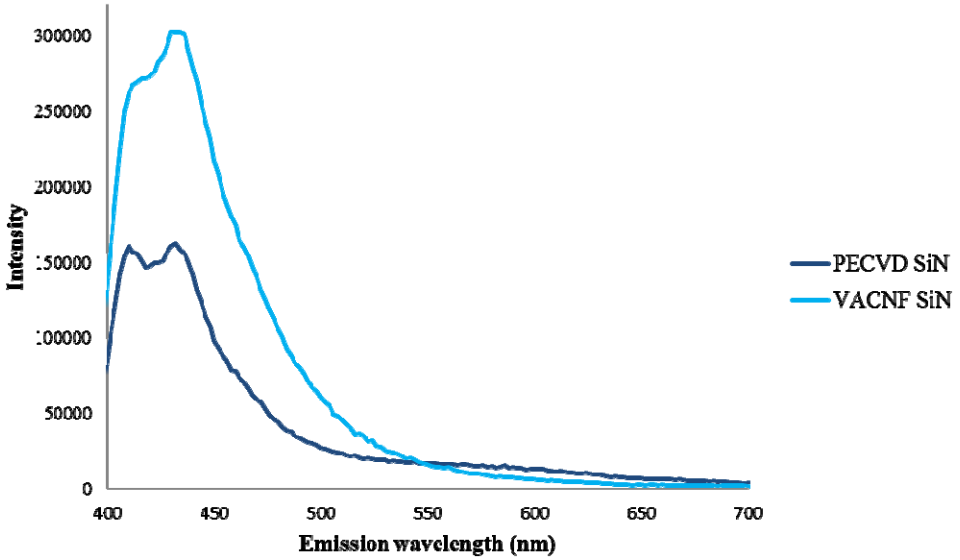


**Figure 5. PL spectra at 380nm excitation for VACNF $SiN_x$ and PECVD $SiN_x$.**

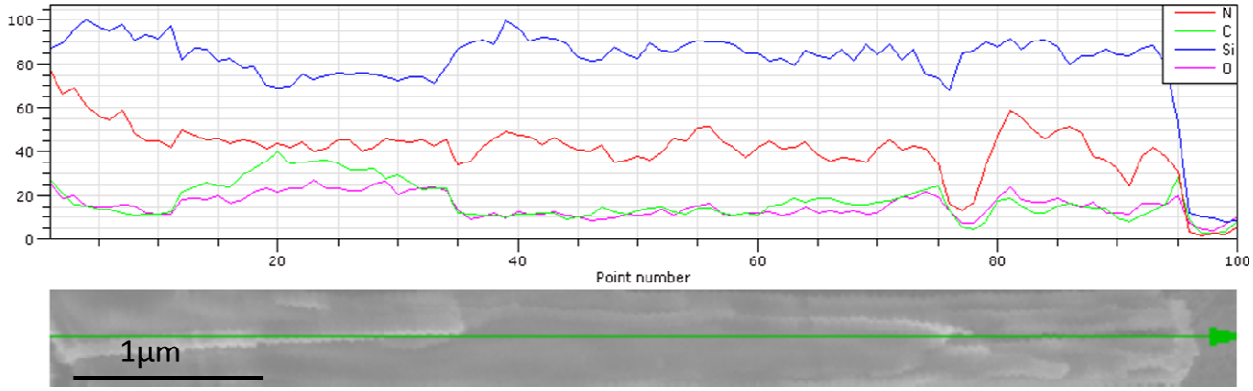


**Figure 6. EDS line scan of a broken VACNF coated with $SiN_x$ (top) with positionally accurate SEM image of broken VACNF (bottom).**

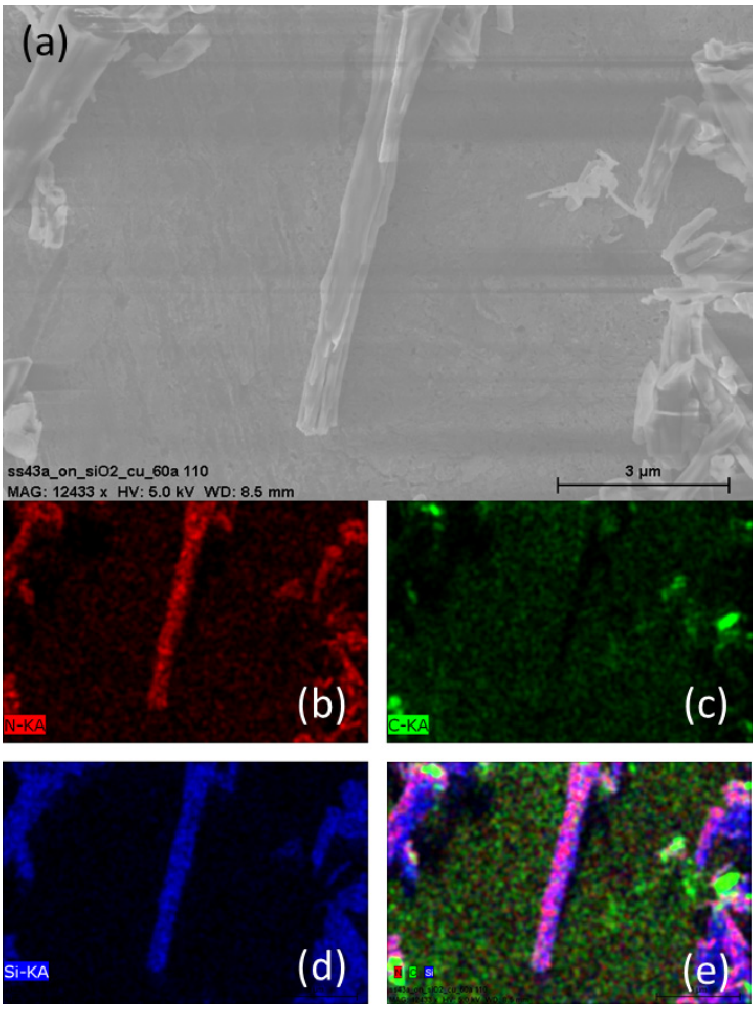


**Figure 7. (a) SEM image of broken VACNFs with $SiN_x$ coatings on an aluminum viewing platform. EDS maps were made of this area showing location of (b) Nitrogen (c) Carbon (d) Silicon and (e) Composite of all three.**

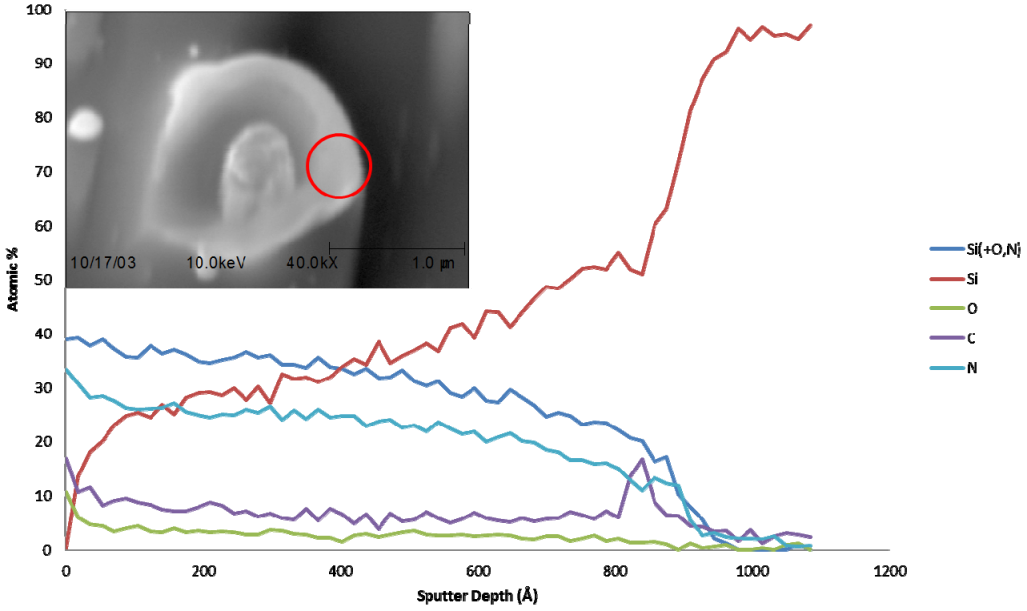


**Figure 8. AES depth profile showing the composition of the $SiN_x$ coating on a VACNF as a function of depth. The inset shows the region that was probed.**

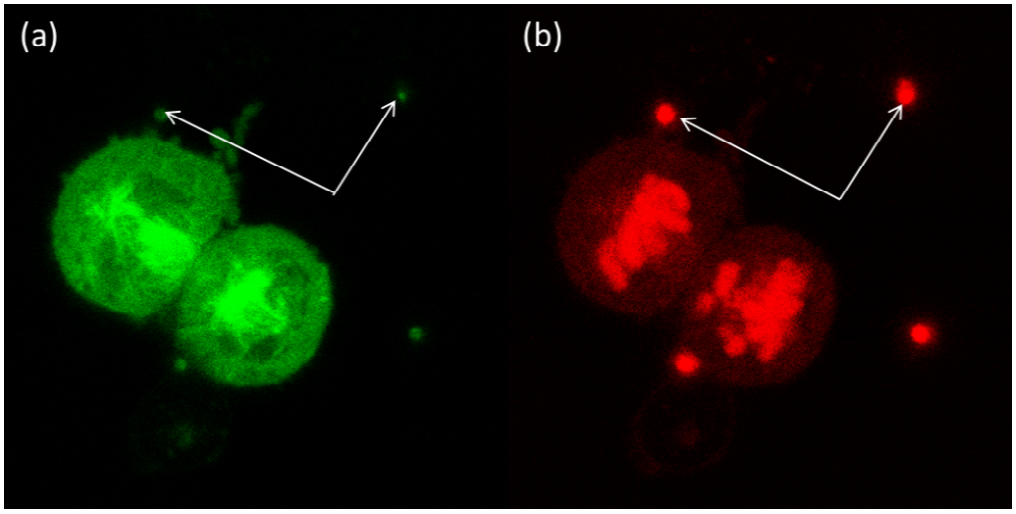


**Figure 9. Fluorescent optical micrographs of a cell undergoing mitosis looking at different emission wavelengths. (a) Emission of 510 nm-520 nm from GFP-tubulin (b) Emission of 600 nm – 655 nm from H2B-DsRed. Arrows indicate location of $SiN_x$ coated VACNFs from a top-down view. The VACNFs are not stained or modified with dye in any way. The nanofibers are on a 5 um × 5 um grid as scale markers.**

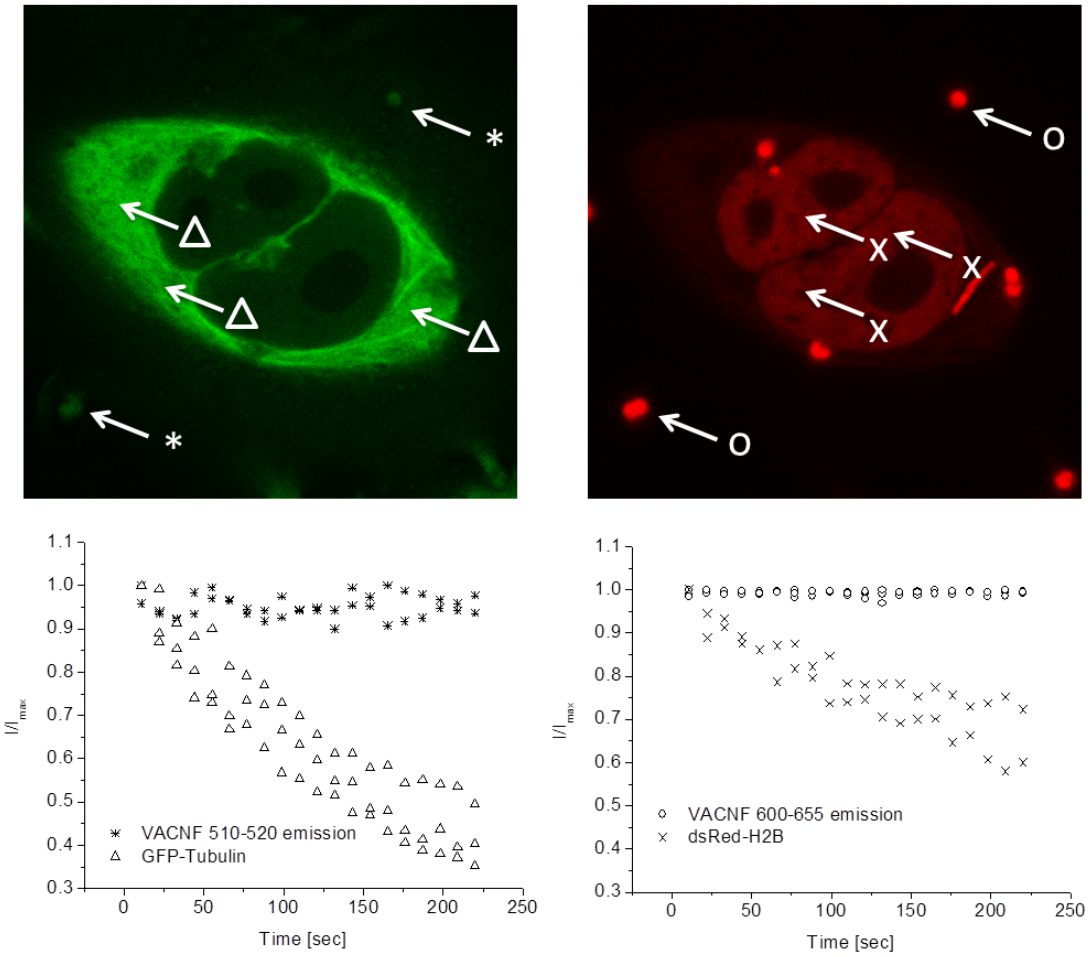


**Figure 10. Fluorescent optical micrographs (top) showing a human osteosarcoma U2OS cell impaled on a $SiN_x$ coated VACNF array following impalefection-mediated delivery of genes encoding GFP-tubulin (left) and H2B-dsRed (right). Graphs indicate the change of the fluorescent intensity (I/Imax) of several regions of interest in each image. Laser excitation at 488 nm for the left set, and 545 nm for the right set causes photobleaching of the transgenic fluorescent proteins, but the nanofiber positions remain virtually unchanged over the duration of imaging. The nanofibers are spaced 5 micrometers apart as scale markers.**

## 4. Conclusion

Here we have proposed a potential mechanism for deposition of $SiN_x$ coating on the sidewalls of VACNFs during PECVD synthesis in addition to exploring the origin of the coating's fluorescence. It seems most likely that the substrate reacts with the process gases through mechanisms similar to reactive sputtering and CVD to form silane and other silicon bearing compounds before being deposited isotropically as a $SiN_x$ coating onto the VACNFs. The case for the presence of Si-NCs is

made strong through a combination of the strong fluorescence and elemental analysis of the samples. These broadly-across the whole visible range-luminescent fibers can prove useful as registry markers in fluorescent cellular studies.

**Acknowledgement**

A portion of research was conducted at the Center for Nanophase Materials Sciences, which is sponsored at Oak Ridge National Laboratory by the Scientific User Facilities Division, Office of Basic Energy Sciences, U.S. Department of Energy.

**References**

1. McKnight TE, Melechko AV, Griffin GD, et al. (2003) Intracellular integration of synthetic nanostructures with viable cells for controlled biochemical manipulation. *Nanotechnology* 14 (5): 551-556.
2. Guillorn MA, Melechko AV, Merkulov VI, et al. (2001) Operation of a gated field emitter using an individual carbon nanofiber cathode. *Appl Phys Lett* 79(21): 3506-3508.
3. Melechko AV, McKnight TE, Hensley DK, et al. (2003) Simpson, Large-scale synthesis of arrays of high-aspect-ratio rigid vertically aligned carbon nanofibres. *Nanotechnology* 14(9): 1029-1035.
4. Teo KBK, Chhowalla M, Amaratunga GAJ, et al. (2002) Characterization of plasma-enhanced chemical vapor deposition carbon nanotubes by Auger electron spectroscopy. *J Vac Sci Technol B* 20(1): 116-121.
5. Yang X, Guillorn MA, Austin D, et al. (2003) Fabrication and Characterization of Carbon Nanofiber-Based Vertically Integrated Schottky Barrier Junction Diodes. *Nano Lett* 3(12): 1751-1755.
6. Pearce RC, Railsback JG, Anderson BD, et al. (2013) Transfer of Vertically Aligned Carbon Nanofibers to Polydimethylsiloxane (PDMS) While Maintaining their Alignment and Impalefection Functionality. *Acs Appl Mater Interfaces* 5: 878-882.
7. McKnight TE, Melechko AV, Austin DW, et al. (2004) Microarrays of vertically-aligned carbon nanofiber electrodes in an open fluidic channel. *J Phys Chem B* 108(22): 7115-7125.
8. Shi JW, Xu F, Zhou PH, et al. (2013) Refined nano-textured surface coupled with SiNx, layer on the improved photovoltaic properties of multi-crystalline silicon solar cells. *Solid-State Electron* 85: 23-27.
9. Xiao SQ, Xu S, Ostrikov K, (2014) Low-temperature plasma processing for Si photovoltaics. *Mat Sci Eng R* 78: 1-29.
10. Ostrikov K, Neyts EC, Meyyappan M, (2013) Plasma nanoscience: from nano-solids in plasmas to nano-plasmas in solids. *Adv Phys* 62(2): 113-224.

11. McKnight TE, Melechko AV, Hensley DK, (2004) Tracking gene expression after DNA delivery using spatially indexed nanofiber Arrays. *Nano Lett* 4(7): 1213-1219.
12. Melechko AV, Desikan R, McKnight TE, et al. (2009) Synthesis of vertically aligned carbon nanofibres for interfacing with live systems. *J Phys D Appl Phys* 42(19): 193001.
13. Melechko AV, Klein KL, Fowlkes JD, et al. (2007) Simpson, Control of carbon nanostructure: From nanofiber toward nanotube and back. *J Appl Phys* 102(7): 074314-7.
14. Chhowalla M, Teo KBK, Ducati C, et al. (2001) Growth process conditions of vertically aligned carbon nanotubes using plasma enhanced chemical vapor deposition. *J Appl Phys* 90(10): 5308-5317.
15. Arumugam PU, Chen H, Siddiqui S, et al. (2009) Wafer-scale fabrication of patterned carbon nanofiber nanoelectrode arrays: A route for development of multiplexed, ultrasensitive disposable biosensors. *Biosens Bioelectron* 24(9): 2818-2824.
16. Serikawa T, Okamoto A, (1984) Properties of Magnetron–Sputtered Silicon Nitride Films. *J Electrochem Soc* 131(12): 2928-2933
17. Benami A, Santana G, Monroy BM, et al. (2007) Visible photoluminescence from silicon nanoclusters embedded in silicon nitride films prepared by remote plasma-enhanced chemical vapor deposition. *Physica E* 38: 148-151.
18. Benami A, Santana G, Ortiz A, et al. (2007) Strong white and blue photoluminescence from silicon nanocrystals in SiN x grown by remote PECVD using SiCl 4 /NH 3. *Nanotechnology* 18(15): 155704.
19. Bommali RK, Singh SP, Rai S, et al. (2012) Excitation dependent photoluminescence study of Si-rich a-SiNx: H thin films. *J Appl Phys* 112(12): 123518-123518-6
20. Brewer A, von Haeften K, (2009) In situ passivation and blue luminescence of silicon clusters using a cluster beam/H2O codeposition production method. *Appl Phys Lett* 94(26): 261102-261102-3.
21. Chopra S, Gupta RP, Joshi BC, et al. (2009) Study of hydrogen passivation in SiNx:H films using Fourier transform infrared and photoluminescence spectroscopy. *Mater Sci P* 27(2): 559-568.
22. Kim BH, Cho CH, Kim TW, et al. (2005) Photoluminescence of silicon quantum dots in silicon nitride grown by $NH_3$ and $SIH_4$. *Appl Phys Lett* 86(9): 091908.
23. Kim TY, Park NM, Kim KH, et al. (2004) Quantum confinement effect of silicon nanocrystals in situ grown in silicon nitride films. *Appl Phys Lett* 85(22): 5355-5357.
24. Kistner J, Chen X, Weng Y, et al. (2011) Photoluminescence from silicon nitride-no quantum effect. *J Appl Phys* 110: 023520.
25. Lopez-Suarez A, Fandino J, Monroy BM, et al. (2008) Study of the influence of $NH_3$ flow rates on the structure and photoluminescence of silicon-nitride films with silicon nanoparticles. *Physica E* 40(10): 3141-3146.

26. Ma K, Feng JY, Zhang ZJ, (2006) Improved photoluminescence of silicon nanocrystals in silicon nitride prepared by ammonia sputtering. *Nanotechnology* 17(18): 4650.
27. Nguyen PD, Kepaptsoglou DM, Ramasse QM, et al. (2012) Direct observation of quantum confinement of Si nanocrystals in Si-rich nitrides. *Phys Rev B* 85(8): 085315.
28. Cho CH, Kim BH, Kim TW, et al. (2005) Effect of hydrogen passivation on charge storage in silicon quantum dots embedded in silicon nitride film. *Appl Phys Lett* 86(14): 143107.
29. Pei Z, Hwang HL, (2003) Formation of silicon nano-dots in luminescent silicon nitride. *Appl Surf Sci* 212-213: 760-764.
30. Santana G, Monroy BM, Ortiz A, et al. (2006) Influence of the surrounding host in obtaining tunable and strong visible photoluminescence from silicon nanoparticles. *Appl Phys Lett* 88(4): 041916.
31. Wang MH, Li DS, Yuan Z, et al. (2007) Photoluminescence of Si-rich silicon nitride: Defect-related states and silicon nanoclusters. *Appl Phys Lett* 90(13): 131903.
32. Hao HL, Wu LK, Shen WZ, et al. (2007) Origin of visible luminescence in hydrogenated amorphous silicon nitride. *Appl Phys Lett* 91(20): 201922.
33. Mann DGJ, McKnight TE, McPherson JT, et al.(2008) Inducible RNA interference-mediated gene silencing using nanostructured gene delivery arrays. *ACS Nano* 2(1): 69-76.
34. Hensley DK, Melechko AV, Ericson MN, et al. (2010) Transparent microarrays of vertically aligned carbon nanofibers as a multimodal tissue interface. Biomedical Sciences and Engineering Conference (BSEC).